Watching Ripples on Crystals

Y. Sugawara,[1] O. B. Wright,[1,*] O. Matsuda,[1] M. Takigahira,[1] Y. Tanaka,[1] S. Tamura,[1] and V. E. Gusev[2]

[1]*Department of Applied Physics, Faculty of Engineering, Hokkaido University, Sapporo 060-8628, Japan*

[2]*Université du Maine, Avenue O. Messiaen, 72085 Le Mans, Cedex 09, France*

(Received 26 December 2001; published 18 April 2002)

We present a new method for imaging surface phonon focusing and dispersion at frequencies up to 1 GHz that makes use of ultrafast optical excitation and detection. Animations of coherent surface phonon wave packets emanating from a point source on isotropic and anisotropic solids are obtained with micron lateral resolution. We resolve rounded-square shaped wave fronts on the (100) plane of LiF and discover isolated pockets of pseudosurface wave propagation with exceptionally high group velocity in the (001) plane of TeO_2. Surface phonon refraction and concentration in a minute gold pyramid is also revealed.

DOI: 10.1103/PhysRevLett.88.185504 PACS numbers: 63.20.Dj, 62.65.+k, 68.35.Iv, 77.65.Dq

Sound waves in crystals, dependent on the fourth-order elastic constant tensor, display a rich array of anisotropic propagation phenomena. Despite a crystal being homogeneous, a point acoustic source in the bulk can lead to singularities in acoustic flux in certain directions owing to the angular dependence of the phase and group velocities of the three acoustic polarizations [1]. This phonon focusing effect was first discovered in the bulk [2], but surface phonons were predicted to produce equally intriguing focusing patterns [3]. In the 10 MHz–1 GHz range, where acoustic wavelengths are typically 3–300 μm, various methods have been suggested for two-dimensional surface phonon imaging, such as stroboscopic probing, the sprinkling of powder on the surface, or detection by immersed point-focus transducers [4–6]. However, despite the growing interest in the field of surface acoustic wave devices, no technique has been successful in imaging surface phonon focusing in real time. Such imaging allows direct access to the dispersion characteristics of the wave propagation and the possibility of following the temporal evolution of cuspidal structures. In this Letter we image the propagation of coherent surface phonons at frequencies up to 1 GHz in real time, allowing animations of point-excited surface phonon wave packets to be made with picosecond temporal and micron spatial resolutions.

We use an ultrafast optical pump and probe technique with a common-path interferometer [7]. Surface phonon wave packets are thermoelastically excited in thin metal films on transparent substrates with optical pulses of wavelength 415 nm, repetition rate 80 MHz (one pulse every 12.5 ns), duration ~1 ps, and pulse energy ~0.3 nJ, producing a maximum transient temperature rise ~100 K. This pump light is focused at normal incidence through the substrate to a circular spot of diameter $D \approx 2$ μm (full width at half maximum intensity; see Fig. 1). Out-of-plane (z) surface motion is detected interferometrically with ~1 pm resolution by the use of two probe pulses at an interval of $\tau = 510$ ps, focused at normal incidence to a single spot of diameter ~D on the front surface of the film. These pulses, of wavelength 830 nm, are derived from the same laser as the pump. In a simple modification of the apparatus of Ref. [7], we divide the output beam from the interferometer into two using a polarizing beam splitter and thereby directly subtract the optical phase ϕ of the probe beams using the difference in the signals from two photodetectors [8]. The relative position of the pump and probe spots is scanned (with ~200 × 200 pixels taking ~8 min per image) at a fixed pump-probe delay time, and this delay is then varied in steps of ~500 ps to produce a full 12.5 ns animation of ~25 frames with a lateral resolution ~D. We mainly use gold films for which ϕ is

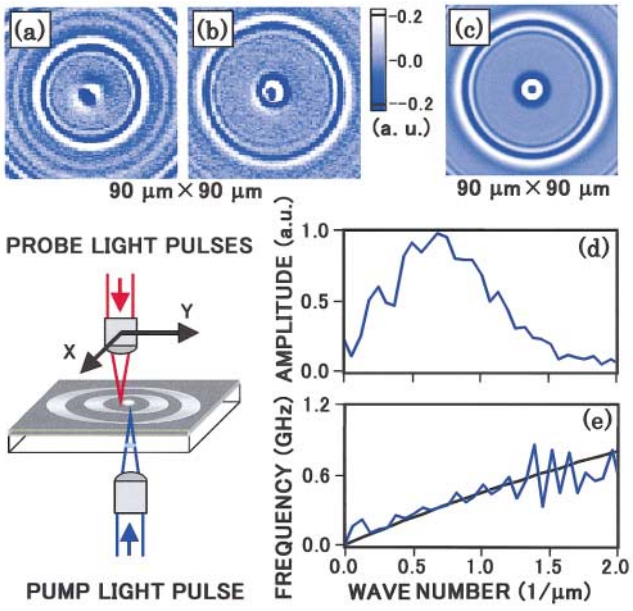

FIG. 1 (color). Data and theory for surface phonon propagation on isotropic crown glass coated with a 70 nm Au film. (a),(b) Experimental surface phonon images at delay times ~10.4 and ~14.2 ns after pump pulse arrival, respectively. The white color corresponds to outward v_z. (c) A simulated image fitted to Fig. 1(b) from the experimental wave vector spectrum $|F_0(k)|$ and the calculated dispersion relation $f = \omega(k)/2\pi$. (d) $|F_0(k)|$. (e) Experimental (blue) and theoretical (black) curves for $f = \omega(k)/2\pi$. Inset: basic imaging apparatus.

sensitive to the out-of-plane surface motion (of amplitude ~20 pm) [7], and so our differential detection technique is essentially imaging the surface particle velocity v_z (since $\tau \ll 1/f$, $f = \omega/2\pi$ the phonon frequency).

Results were first obtained for an isotropic material: a crown-glass substrate of thickness 1 mm coated with a 70 nm polycrystalline gold film. Figures 1(a) and 1(b) show two frames of an animation for a 90 μm × 90 μm region at fixed delay times 10.4 and 1.7 ns (equivalent to 1.7 + 12.5 = 14.2 ns), respectively (measured between pump and average probe pulse arrival). Multiple expanding circular wave fronts, reminiscent of ripples on water [9], arise because of the periodic excitation and the elastic isotropy. The feature at the center of the images is due to thermal expansion [10].

For quantitative analysis we take the two-dimensional spatial Fourier transform $F(\mathbf{k}, t)$ ($\mathbf{k}$ is the 2D wave vector) of the time-dependent coherent surface disturbance $f(\mathbf{r}, t)$, a real function, where $f(\mathbf{r}, t)$ represents the experimental difference in ϕ:

$$f(\mathbf{r}, t) = \int_{-\infty}^{\infty} F(\mathbf{k}, t) \exp[i\mathbf{k} \cdot \mathbf{r}]\, d^2\mathbf{k}$$

$$= \mathrm{Re} \int_{-\infty}^{\infty} F_0(\mathbf{k}) \exp[i(\mathbf{k} \cdot \mathbf{r} - \omega(\mathbf{k})t)]\, d^2\mathbf{k}\,, \quad (1)$$

$$F(\mathbf{k}, t) = \tfrac{1}{2}\{F_0(\mathbf{k}) \exp[-i\omega(\mathbf{k})t] + F_0^*(-\mathbf{k}) \exp[i\omega^*(-\mathbf{k})t]\}, \quad (2)$$

where the wave propagation is assumed to be governed by a single mode and by a linear wave equation that may in general include loss terms. If three consecutive $F(\mathbf{k}, t)$ at constant interval t_1 are known (with the central time defined here as $t = 0$), the use of Eq. (2) allows us to obtain $\omega(\mathbf{k})$:

$$\cos[\omega(\mathbf{k})t_1] = \frac{F(\mathbf{k}, -t_1) + F(\mathbf{k}, t_1)}{2F(\mathbf{k}, 0)}\,, \quad (3)$$

provided that (i) $\omega(\mathbf{k}) = \omega^*(\mathbf{k})$, implying negligible acoustic attenuation, and (ii) $\omega(\mathbf{k}) = \omega(-\mathbf{k})$, implying a laterally homogeneous sample. These two conditions are satisfied for our probed areas. Equation (3) gives $\omega(\mathbf{k})$ for a single mode from three images of $f(\mathbf{r}, t)$.

Figures 1(d) and 1(e) show $|F_0(k)|$ and $\omega(k)/2\pi$ (in blue) derived from Eqs. (2) and (3) using the average of the derived function $\omega(\mathbf{k})$ for $\mathbf{k}$ in the x and y directions [11]. Phonon wavelengths Λ in the range 3 to 30 μm (frequencies $f \sim 100$ MHz to 1 GHz) are excited, with a peak at 9 μm ($f \sim 350$ MHz). This agrees with rough estimates based on the optical spot size ($\Lambda \gtrsim D$) and mode velocity (3000 ms^{-1}). The black curve in Fig. 1(e) shows the result of an analytical calculation for the dispersion of the first Rayleigh-like mode [12]. The slight curvature due to film loading is consistent with the experimentally derived result (within the range of k that are significantly excited). A more stringent test of this theory is shown by the image in Fig. 1(c). This represents a simulation on

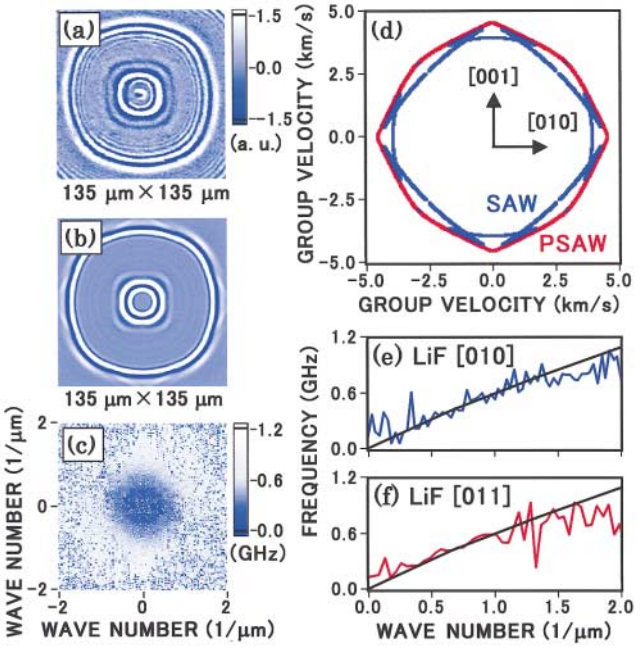

FIG. 2 (color). Data and theory for surface phonon propagation on cubic LiF(100) coated with a 50 nm Au film. (a) Experimental surface phonon image at delay time ~3.7 ns. (b) A FDTD simulation image without the Au film. (c) Dispersion image $f = \omega(\mathbf{k})/2\pi$ obtained from three images at 400 ps intervals. (d) Theoretical group velocities for SAW (blue) and PSAW (red). (e),(f) Dispersion relations (cross sections of the dispersion image) for the [010] and [011] directions. The smooth curves are theoretical predictions.

the basis of Eq. (1), which makes use of the theoretically calculated $\omega(k)$ and a fit to the experimental $|F_0(k)|$ [13]. The agreement with experiment is excellent [see Fig. 1(b)], justifying the assumptions made in the analysis.

We now turn to anisotropic samples. We chose LiF as a cubic crystal which, from a consideration of ratios of its elastic constants alone, is expected to have a folded group velocity surface with fourfold symmetry and to show surface phonon focusing [14]. Figure 2(a) shows a 135 μm × 135 μm surface phonon image for the (100) surface of LiF of thickness 1 mm coated with a 50 nm polycrystalline gold film. The x and y axes correspond to [010] and [001], respectively. Strikingly, the phonon wave fronts are rounded square shapes. In order to reproduce this behavior theoretically, the elastic wave equation with free surface boundary conditions is numerically solved for the surface particle velocity v_z using the finite-difference time-domain (FDTD) method for the substrate alone [15]; Fig. 2(b) shows the simulated image for two consecutive pump pulses. The finer ripples in experiment are not reproduced owing to the neglect of the film loading, but the agreement is reasonable. Recall that Rayleigh waves penetrate to a depth ~Λ [16], and so a film that is very thin in comparison will have a small perturbing effect. The FDTD simulation does not clearly distinguish different acoustic modes, so we have carried out an analytical calculation of the direction-dependent group velocities: Fig. 2(d) shows

the results for surface acoustic waves (SAW, in blue), exhibiting characteristic cusps, and pseudosurface acoustic waves (PSAW, in red). PSAW behave like SAW, with a higher phase velocity than SAW for a given direction, though they are not true (nondecaying) surface waves, having a quasitransverse bulk wave component with propagation vector tilted down into the solid [3,14]. By comparison of Figs. 2(b) and 2(d) we see that the SAW component is dominant for angles within ~25° to the [010] directions, whereas the PSAW component is dominant for angles within ~20° to the [011] directions. It is a remarkable coincidence that these two modes are beautifully and smoothly combined at intermediate angles as if only one mode were present.

This suggests that our previous single-mode analysis might allow the derivation of a meaningful "dispersion image": Fig. 2(c) shows $f = \omega(\mathbf{k})/2\pi$ obtained from Eq. (3) with the single-mode assumption. We concentrate on representative propagation directions in which the acoustic flux is focused. The blue curve in Fig. 2(e) is the average obtained from the x and y sections of Fig. 2(c), corresponding to the [010] dispersion relation; the black curve is a result of an analytical calculation for SAW including film loading. The red curve in Fig. 2(f) is the average of diagonal sections of Fig. 2(c), corresponding to the [011] dispersion relation; the black curve is the result of an analytical calculation for this direction including film loading. The experimental dispersion curves for these directions are in good agreement with the theory. This is not unexpected because for the directions chosen only a single mode is excited. [Owing to the success of the single-mode analysis here, we have not attempted to extend the approach of Eqs. (1)–(3) to two modes using a process that would require six images.]

Rather than pursuing at this stage other cubic crystalline cuts or different cubic crystals, we have imaged TeO_2, a tetragonal crystal with much stronger anisotropy [17]. Figure 3(a) shows a 150 μm × 150 μm surface phonon image for the (001) surface of single-crystal TeO_2 of thickness 1 mm coated with a 40 nm polycrystalline gold film. The x and y axes correspond to [100] and [010], respectively. The pattern is exquisitely intricate owing to the anisotropy and the repeated pulsed excitation and shows the expected fourfold symmetry for this cut. Figure 3(b) shows an image of v_z based on a FDTD simulation for the bare substrate, corresponding to the second excited phonon wave packet from the center in Fig. 3(a) [18]. The wave front shape is in good agreement with experiment. Figure 3(c) shows the result of analytical calculations of the group velocities of SAW (in blue), PSAW (in red), and longitudinal bulk waves (in green) for the (001) surface of TeO_2, ignoring film loading. Various comparisons can be made. (i) The complicated wave fronts in experiment arise from the strong anisotropy and resulting caustic behavior evident in the group velocity predictions. (ii) Some of the calculated wave fronts are not observed because of the combined effects of phonon focusing and the selective v_z detection.

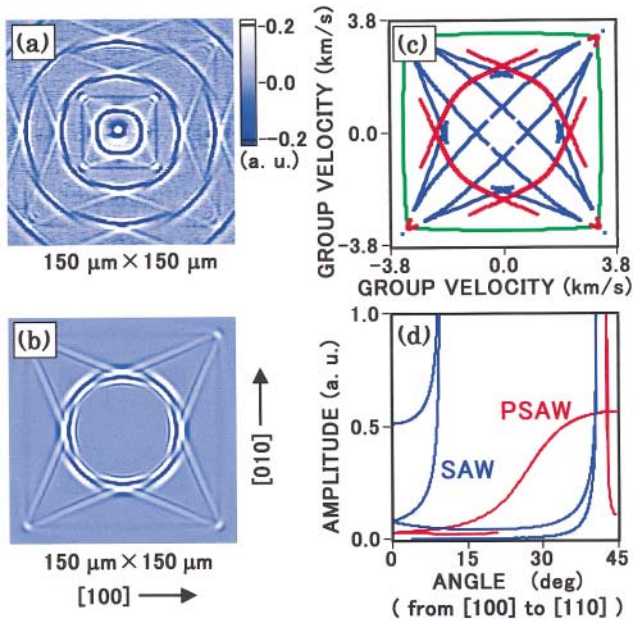

FIG. 3 (color). Data and theory for surface phonon propagation on tetragonal TeO_2(001) coated with a 40 nm Au film. (a) Experimental surface phonon image at delay time ~8.0 ns. (b) A FDTD simulation image without the Au film. (c) Theoretical group velocities for SAW (blue), PSAW (red), and longitudinal bulk waves (green). (d) Amplitude (weighted by the density of the group velocity vectors) corresponding to the vertical component of the surface velocity for SAW (blue) and PSAW (red) as a function of propagation angle. The ratio of the scales for SAW and PSAW is arbitrary.

This is confirmed from calculations of the angular dependence of the v_z signal amplitude for point excitation, as shown in Fig. 3(d) for each mode. The PSAW and SAW wave fronts *not* observed correspond to the crossed red curves (in the 0° to ~ ±17° range measured from [100]) and the diagonal blue curves, respectively, in Fig. 3(c). This is consistent with Fig. 3(d). (iii) In Fig. 3(a), in particular near the center, the square wave fronts correspond to those predicted for longitudinal bulk waves (in green). Representative sound velocities estimated from experiment are ~4.4 km s^{-1} for [110] propagation and ~3.2 km s^{-1} for [100], compared to the calculated bulk values 4.46 km s^{-1} and 3.32 km s^{-1}, respectively. The experimental square wave fronts are therefore likely to represent the effect of longitudinal bulk waves propagating parallel to the surface, and indeed these are faintly visible in Fig. 3(b). (iv) Isolated PSAW pockets predicted near the corners of Fig. 3(c) are clearly resolved in experiment and in the simulation. Counterintuitively, these PSAW have a group velocity ~4.5 km s^{-1}, faster than any bulk modes with wave vectors lying in the (001) plane [19]. Experimental dispersion analysis for TeO_2 is not trivial, owing to the overlapping wave fronts, and is beyond the scope of this Letter.

Our final sample is a microstructure with lateral inhomogeneity. Figure 4(a) shows a 90 μm × 90 μm surface phonon image and Fig. 4(b) shows an optical reflectivity

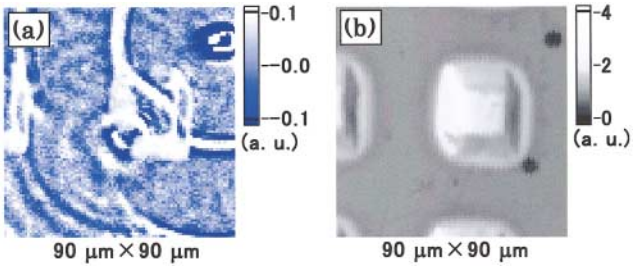

FIG. 4 (color). Experimental images for a crown-glass substrate coated with a 140 nm Cr film and Au pyramids of height 1 μm. (a) Experimental surface phonon image at delay time 0.5 ns. (b) Optical reflectivity image of the same region. The pump pulses are incident at the top right.

image (at the probe wavelength), obtained simultaneously for the same region. The pump pulses are incident at the top right. To make the sample a 140 nm polycrystalline chromium film was prepared by electron beam deposition on a 1 mm crown-glass substrate. Polycrystalline gold of thickness 1 μm was then thermally evaporated through a mask consisting of a grid of 25 μm $\times$ 25 μm square holes of separation 60 μm. This mask was not flush with the substrate, leading to a smearing of the Au pattern to produce an array of flat-topped Au pyramids. The whiter regions in Fig. 4(b) correspond to Au and the darker region to Cr [20]. The difference in SAW propagation velocities in Au (1.13 km s^{-1}) and in crown glass (3.1 km s^{-1}) is mainly responsible for the refraction at the pyramid boundaries, producing an inversion of the wave front curvature inside the pyramid. The SAW are thus concentrated and are strongly scattered on exiting. We have not attempted a numerical simulation of this system, which should ideally take account of the pyramid's three-dimensional shape.

In conclusion, we have demonstrated a method for real-time imaging of coherent surface phonons. Direct dynamic visualization of phonon wave fronts is not only a delight to behold, but it provides new insights into the elaborate underlying mechanisms for phonon focusing, dispersion, refraction, and scattering and can reveal the details of the modal structure. In the future it will be straightforward to modify the technique for application to opaque substrates. This research should therefore open the way to a wide variety of studies in surface-phonon "optics" involving the animation of phonon ripples on samples as diverse as surface phononic crystals, phonon waveguides, and phonon resonators. Moreover, there are intriguing possibilities for interdisciplinary studies on materials exhibiting strong magnetoelastic or piezoelectric effects or, at higher acoustic intensities, for the tracking of acoustic soliton propagation.

*Corresponding author.
Email address: assp@kino-ap.eng.hokudai.ac.jp

[1] J. P. Wolfe, *Imaging Phonons* (Cambridge University Press, Cambridge, U.K., 1998).
[2] B. Taylor, H. J. Maris, and C. Elbaum, Phys. Rev. B **3**, 1462 (1971).
[3] S. Tamura and K. Honjo, Jpn. J. Appl. Phys. Suppl. 3 **20**, 17 (1980); R. E. Camley and A. A. Maradudin, Phys. Rev. B **27**, 1959 (1983); A. G. Every, Phys. Rev. B **33**, 2719 (1986).
[4] M. Clark, S. Sharples, and M. Somekh, Meas. Sci. Technol. **11**, 1792 (2000).
[5] A. A. Kolomenskii and A. A. Maznev, Phys. Rev. B **48**, 14 502 (1993).
[6] R. E. Vines, S. Tamura, and J. P. Wolfe, Phys. Rev. Lett. **74**, 2729 (1995).
[7] D. H. Hurley and O. B. Wright, Opt. Lett. **24**, 1305 (1999).
[8] The polarizing beam splitter, inserted with axes at 45° to the plane of the interferometer, replaces a final polarizer.
[9] The dispersion $\partial^2\omega/\partial k^2 < 0$ here is of the opposite sign to that of water ripples. See C. A. Coulson, *Waves* (Oliver and Boyd, Edinburgh, U.K., 1961).
[10] O. B. Wright and K. Kawashima, Phys. Rev. Lett. **69**, 1668 (1992).
[11] A window function is used to select a single circular phonon wave packet in three images spaced by 400 ps, centered at a time 14.2 ns after excitation.
[12] G. W. Farnell and E. L. Adler, in *Physical Acoustics,* edited by W. P. Mason and R. N. Thurston (Academic, New York, 1972), Vol. 9, p. 35. The elastic constants are taken as $c_{11} = 207$ GPa, $c_{44} = 28.5$ GPa, and the density as $\rho = 19.32$ g cm^{-3} for the gold film; $c_{11} = 81.5$ GPa, $c_{44} = 29.3$ GPa, and $\rho = 2.55$ g cm^{-3} for crown glass.
[13] We use $F_0(\mathbf{k}) = F_0(k) = i[1 - \exp(-2k/\Delta k)]\exp[-(k - k_0)^2/(\Delta k)^2]$ in the simulation, with $k_0 = 2\pi/15$ μm^{-1} and $\Delta k = 2\pi/8$ μm^{-1}. Here $t = 0$ for the pump pulse arrival time. We assume spatial symmetry of the source, so $F_0(\mathbf{k}) = F_0(-\mathbf{k})$, and *temporal* symmetry in the outward surface *displacement* about $t = 0$, so $F_0(-\mathbf{k}) = -F_0^*(\mathbf{k})$. The function $|F_0(k)|$ is a fit to the experimental curve in Fig. 1(d).
[14] A. A. Maznev and A. G. Every, Acta Acust. (France) **1**, 137 (1994).
[15] See A. Tavlove, *The Finite-Difference Time-Domain Method* (Artech House, Boston, 1998). The grid size used is $\Delta x = \Delta y = \Delta z = 0.33$ μm and $\Delta t = 2.1$ ps. The parameters used for $F_0(\mathbf{k}) = F_0(k)$ are slightly different from before owing to a slightly larger spot size: $k_0 = 2\pi/25$ μm^{-1} and $\Delta k = 2\pi/9$ μm^{-1}. Initial conditions for surface displacement consistent with $F_0(k)$ were used. For LiF we take $c_{11} = 111.2$ GPa, $c_{12} = 42.0$ GPa, and $c_{44} = 62.8$ GPa, and $\rho = 2.639$ g cm^{-3}.
[16] Lord Rayleigh, Proc. London Math. Soc. **17**, 4 (1885).
[17] D. C. Hurley, J. P. Wolfe, and K. A. McCarthy, Phys. Rev. B **33**, 4189 (1986).
[18] For $F_0(\mathbf{k}) = F_0(k)$ we take the same parameters as for crown glass, noting that the thermal expansion tensor is isotropic in the (001) plane for TeO_2. We take $c_{11} = 55.7$, $c_{12} = 51.2$, $c_{13} = 21.8$, $c_{33} = 105.8$, $c_{44} = 26.5$, and $c_{66} = 65.9$ (in units of GPa), and $\rho = 5.99$ g cm^{-3}, and ignore small piezoelectric effects.
[19] Isolated solutions for SAW, evident at 45° in Fig. 3(c), are not experimentally resolved.
[20] The pump energy (~0.5 nJ) was higher here, and there is some damage visible in Fig. 4(b).